7ICMSNSE-079

Neutronic characterization of GFR demonstrator

J. Haščík, Š. Čerba, J. Lüley and B. Vrban

Institute of Nuclear and Physical Engineering, Slovak University of Technology in Bratislava, Bratislava, Slovakia

jan.hascik@stuba.sk, stefan.cerba@stuba.sk, jakub.luley@stuba.sk, branislav.vrban@stuba.sk

Abstract

The presented paper is related to introduction of the design and neutronic characterization of the start-up core developed for Gas-cooled Fast Reactor (GFR) demonstrator. The Slovak University of Technology in Bratislava joined the project ALLEGRO in last decade as part of the consortium of middle-European institutions. The reactor core is based on the standard and MOX pin type fuel from the first phase of the project. Neutronic characterization is aimed to determine the standard neutronic parameters using conventional computational systems. Results for the heterogeneous and homogenized designs of the fuel region are presented depending on computational code, cross-section library and energy structure.

Keywords: Neutronics, MOX type fuel, Code Validation, GFR demonstrator

1. Introduction

The Gas-cooled Fast Reactor (hereinafter GFR) is one of the six most promising reactor concepts selected by the Generation IV International Forum (GIF) [1]. –The Sustainable Nuclear Energy Technology Platform (SNETP) has selected the GFR as one of the most suitable reactor designs to deal with the issues of uranium utilization and waste minimization. The design of this reactor may partially benefit from a number of previously proposed but not realized concepts, as well as from the research of technologies related to the sodium cooled fast reactor and the very-high temperature reactor. ALLEGRO, a 75 MW_{th} reactor unit plays a vital role in the development of an electricity producing GFR prototype. As a demonstrator of the unique technology, never built before, it will serve to demonstrate the viability of the GFR system in terms of incorporation, at a reduced scale, of all of the architecture and main materials and components planned for the GFR, except for the power conversion systems. The starting ALLEGRO configuration (hereinafter ALLEGRO MOX) is a qualified technology core characterized by standard Mixed OXide (MOX) sub-assemblies consisting of fuel pins with stainless steel cladding operating at an average coolant temperature around 400 °C [2].

Several neutronic studies are presented, covering criticality, sensitivity, similarity and uncertainty analyses. Detailed SCALE6 KENO VI [3], MCNP5 [4] and DIF3D [5] models have been developed and numerous calculations were performed to determine neutronic parameters, such as k_{eff} , neutron flux spatial distribution, neutron spectra, local multiplicative factors, sensitivity profiles and response uncertainties. Although the main contributors to the development of this reactor are France, UK, Switzerland and Germany, Slovakia has been given the privilege to participate in the research since the ALLEGRO reactor is assumed to be sited in the central European region.

2. General design overview

The ESNII+ ALLEGRO MOX core design is an experimental unit with thermal power of 75 MW $_{\rm th}$. This fast spectrum reactor is a helium-cooled system. The primary coolant pressure reaches 7_MPa during normal operation in order to ensure adequate heat transfer. The three decay heat removal loops with helium-gas heat exchangers are available to mitigate a core melting accident. The global primary arrangement is based on two main helium-water loops (2x38 MW $_{\rm th}$), each fitted with one IHX blower unit. Produced heat is finally transferred by air coolers from the secondary circuit to the atmosphere as the ultimate heat sink. The full core layout and fuel loading pattern of the ALLEGRO MOX reactor core model are shown in Figure 1.

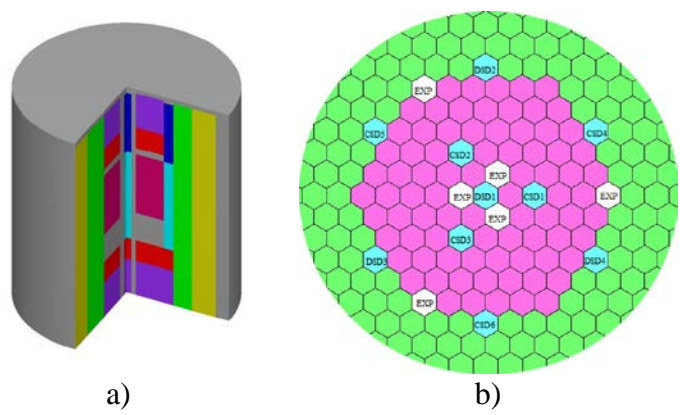


Figure 1 Full core layout and fuel loading pattern of the ALLEGRO MOX core

The 120 degree symmetric core includes 81 fuel sub-assemblies, with 169 fuel pins with the PuO_2 content of the heavy metal material being 25.5% by volume. In addition, the ALLEGRO MOX core features 6 in-core dummy sub-assemblies of dedicated special steel alloy 15-15Ti (AIM1), so far assumed homogeneous in geometry and composition. Figure 1-b) displays a horizontal cross-sectional view of the reference core fuel loading pattern with reflector and shielding subassemblies at the middle active core height. The control rod system is composed of 4 Diverse Shutdown Devices (DSD) and 6 Control and Shutdown Devices (CSD). The absorber rods in both groups are composed of boron carbide. The core fuel region is surrounded by four additional rings of reflector assemblies ($80\%_v$ AIM1 + $20\%_v$ He at 70 bar) in the radial direction and by the 30.2 cm high axial reflectors of almost the same material placed above and below the fission gas plenums. An additional three rings of shielding assemblies are placed around the reflector in the radial direction. Axial shielding placed just under and above the axial reflector region uses a lower proportion of B_4C [2].

3. Computational tools

To ensure diversity of the results, 2 stochastic and 1 deterministic codes were used for this study. As a reference, the MCNP5 [4] code was selected. This code treats an arbitrary three-dimensional configuration of materials in geometric cells and is very versatile in source definition and tally structures. One of the main advantages of MCNP5 is its flexibility to use various pointwise cross section (XS) libraries. On the other hand, the user must pay a "heavy" computational price for the continuous energy (CE) calculations and therefore it is not advantageous to use MCNP5 for routinely repeating calculations. The SCALE6 [3] system solves this issue by introducing a multi-group (MG) approach, in addition to the thorough CE treatment. Although the use of MG treatment can speed up the Monte Carlo (MC) calculation by a factor of several times, the resonance self-shielding of the system

may be influenced or even omitted. In such cases, the physics of the investigated system may be significantly altered. In addition to the MC uncertainty, this may bring another set of discrepancies into the calculations. As a counterweight to these "brute force" stochastic techniques, there are several sophisticated deterministic methods available. These methods solve the Boltzman transport equation directly by means of numerical methods. The majority of deterministic codes are often burdened with limitations. This is reflected in the simplicity of geometry models, or for more complex systems, the transport solution is replaced by diffusion approaches. In either case, the physics of the system should be well understood. DIF3D [5] is a deterministic diffusion code that is capable of solving various geometry structures, including hexagonal 3D problems using the nodal method. It works with regionwise multi-group XS libraries in the ISOTXS format. For this study, 2 sets of XS libraries were used, both prepared using the TRANSX [6] code. The first set was the ZZ_KAFAX_E70 [7], which is a Korean 150 group neutron XS library for fast reactors in MATXS format based on ENDF/B-VII [8] evaluated data. The second set, SBJ_620G_E71, is a 620 group neutron XS library. It was prepared by the authors of this paper for the purpose of GFR reactor core calculations. For both XS libraries, the collapsed 25 group versions were used as well.

4. Computational schemes

The computational scheme for MCNP5 and DIF3D is shown in Figure 2. The scheme for MCNP is quite simple, since the material model of the investigated system is defined within the MCNP input file. It is therefore sufficient to process the ENDF/B-VII evaluated data files to the appropriate ACE continues energy XS library using the NJOY99 [9] code. For the DIF3D code, 2 types of XS data were used in this analysis. In the first case, the fine group SBJ_620G_E71 XS library was prepared using the NJOY99 code. As a source of evaluated data the ENDF/B-VII distribution was used. The average neutron spectrum of the GFR, calculated by MCNP5, was used as a weighting function. The required background XS were taken from the ZZ_KAFAX_E70 library. Using the TRANSX code, 620 group isotope-wise XS were prepared. These XSs were used for the 3D diffusion calculation in DIF3D. Although the 620 group structure is fine enough to account for resonance self-shielding, the large number of energy groups puts significant demand on hardware and considerably extends the calculation time.

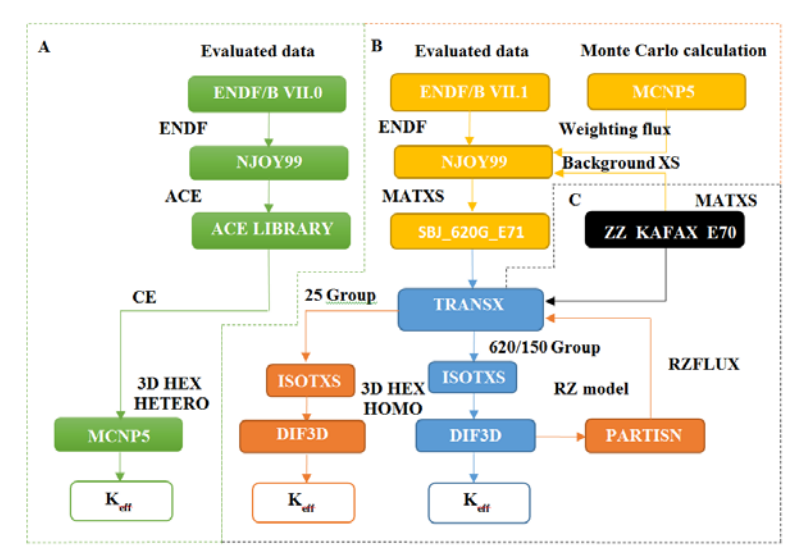


Figure 2 Calculation scheme for the MCNP5 and DIF3D codes

To speed up the DIF3D calculation region dependent fluxes (RZFLUX) were calculated using the RZ model of ALLEGRO. The RZFLUX file was used by the TRANSX code to collapse the group structure from 620 to 25 groups. Finally, the DIF3D calculation was repeated using the new set of XS. In the second DIF3D case, the whole procedure starting from the generation of fine-group ISOTXS libraries was repeated for the ZZ_KAFAX_E70 library. The difference was only in the group collapsing, since in the case of ZZ_KAFAX_E70 the basic data is tabulated in a 150-group structure. For the SCALE6 system it was not necessary to adopt a special scheme for XS processing. For either CE or MG calculations, the code package contains all required information. To generate self-shielded multi-group XS libraries the CENTRM/PMC sequence can be used. However, it is also possible to perform MG Monte Carlo transport without cell calculations.

5. Results

5.1 ALLEGRO MOX core characterization

In terms of the most basic calculation of excess reactivity (ρ_e), there were 11 cases investigated, all of which are listed in Table 1. For MCNP5 and SCALE6 heterogeneous core models were used, but homogenous core models were used for DIF3D. In both cases all control rods were placed at the upper position, marked as "all-up" (AU). The influence of the used XS libraries was estimated by the relative deviation ($\Delta \rho_{MCNP}$) from the MCNP5 CE calculation.

Computer code	XS data file	Energy groups	$ ho_e$ [pcm]	Δho_{MCNP} [pcm]
MCNP5	ENDF/B VII.0	CE	1126.8 ± 7.9	
KENO6	ENDF/B VII.0	CE	1292.5 ± 4.7	165.7
KENO6	ENDF/B VII.0	CE HOMO	974.4 ± 19.6	-152.4
KENO6	ENDF/B VII.0	27 G	6263.5 ± 8.8	5136.7
KENO6	ENDF/B VII.0	200 G	2713.3 ± 8.4	1586.5
KENO6	ENDF/B VII.0	238 G	2870.2 ± 9.4	1743.4
KENO6	ENDF/B VII.0	238 G + cell	2539.1 ± 8.9	1412.3
DIF3D	SBJ_620G_E71	620 G	1089.7	-37.1
DIF3D	ZZ_KAFAX_E70	150 G	512.0	-614.8
DIF3D	SBJ_620G_E71	25 G	1605.5	478.7
DIF3D	ZZ_KAFAX_E70	25 G	1112.8	-14.0

Table 1 Comparison of various XS libraries and group structures.

The results clearly show that the 27 group XS library of KENO6 is not suitable and even the 200 and 238 group structures are significantly overestimating the excess reactivity of the system. The 238 group libraries can be used only if cell calculations are performed, but even in this case the deviation exceeds 1400 pcm. This could be explained by the changes of the neutron spectrum at the boundary of the fuel and reflector. There was a very good agreement found between the CE MCNP5 and fine group DIF3D calculations; for the 620 group case, the deviation was only -37.1 pcm. After transport corrections and group collapsing, the deviation from MCNP5 was still lower than 500 pcm, while the single processor calculation time was decreased to 8.8 seconds (24 hours for MCNP5 on a parallel 12 processor system). After considering all of the advantages and disadvantages, the DIF3D code with both XS libraries and the SCALE6 system with 238 group XS libraries were selected for next calculations. The mean neutron flux energy spectrum for 25 and 150 group structure is presented in Figure 3-a).

To understand the behaviour of the ALLEGRO MOX core from the local point of view, the calculation of local multiplication values (LMV) can be used. These LMV factors may paint out how a given fuel assembly is behaving in a given position of the reactor core. These LMV factors can reveal existence of locally decoupled neutronic zones. These factors were calculated for "all down" (AD) cases. The results can be found in Figure 3-b).

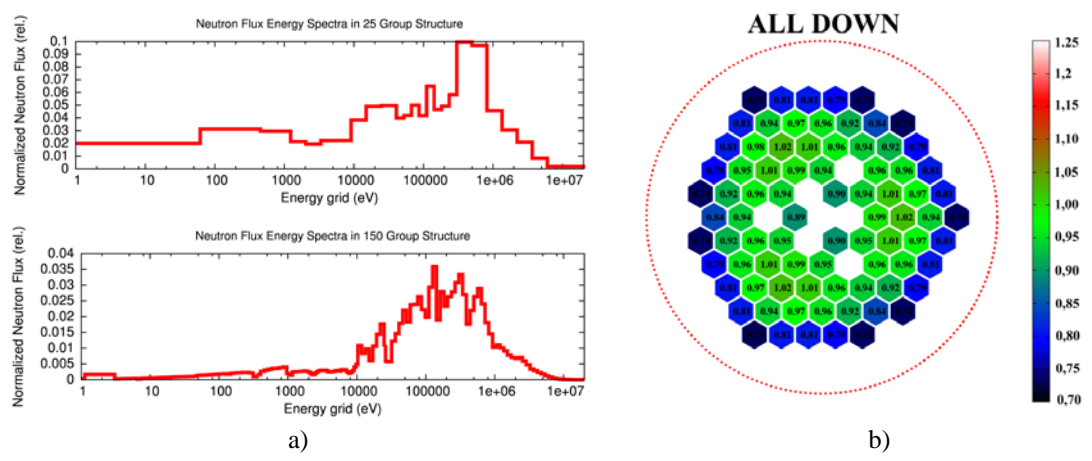


Figure 3 Neutron flux energy spectra and results of LMV factors for "all-down" (AD) case

It is obvious that under normal operation conditions the LMV factors exceed the value of unity, but the issue of concern is the existence of such zones in a case when all of the CRs are fully inserted. From Figure 3-b) we can see 12 S/As with LMV>1 and another 4 where the LMV are close to 1. This phenomenon may have been caused by the low worth of control rods in the peripheral region. This question should be addressed in future analyses.

5.2 Control rod worth

To evaluate whether the system of control rods (CR) disposes enough negative reactivity to bring the reactor to a sufficient level of sub-criticality, the worth of each control rod should be of a high interest. The worth of i-th CR ($\Delta \rho_i$) can be calculated by Eq. (1) where ρ_e is the excess reactivity of the system and ρ_i is the reactivity, when the i-th CR is fully inserted. The results can be found in Table 2.

$$\Delta \rho_i = \rho_i - \rho_e \,. \tag{2}$$

Due to the 120° symmetry of the core, only specific CR positions were investigated. In the reference MCNP5 case, the worth of all of the CR was calculated to 12734.6 ± 11.2 pcm. Due to the distribution of neutron flux in the core, the worth of single devices in various positions differs in a significant way. While the worth of the central DSD1 device was 2599.1 ± 5.5 pcm, the peripheral CSD4 unit disposes only 452.6 ± 5 pcm. Although there were appreciable discrepancies in the calculation of excess reactivity between codes and XS libraries, these tendencies were also consistent for cases with inserted CR and therefore the deviations in the CR worth were not that significant. For the case with all CR inserted in the core, marked as "all-down" (AD), there was a -135 pcm deviation between MCNP5 and SCALE6 and 800 pcm deviation between MCNP5 and DIF3D. For single CRs this discrepancy did not exceed 2 %. This accuracy is sufficient, since in MCNP5 the heterogeneous CR design was investigated, while in DIF3D homogeneous compositions were used. The discrepancy between the two DIF3D calculations can be considered negligible. All of the data discussed is summarized in following table.

Table 2 Results of control rod worth

Control and ID	SCALE6	MCNP5	DIF	F3D
Control rod ID	E70 235G	E70 CE	KAFAX_E70	SBJ_E71
AD	12599.2 ± 7.2	12734.6 ± 11.2	11565.4	11800.6
CSD1	2286.7 ± 5.4	2310.0 ± 11.3	2172.4	2199.6
CSD4	452.6 ± 5.4	442.9 ± 11.1	436.5	451.5
DSD1	2599.1 ± 5.5	2643.9 ± 11.4	2342.3	2397.1
DSD2	451.6 ± 5.4	447.8 ±11.1	451.5	451.5
CSD	8871.1 ± 4.2	8952.2 ± 11.1	8278.7	8424.3
DSD	4111.8 ± 4.2	4130.8 ± 11.2	3754.3	3863.3
CSD1R	7239.8 ± 5.6	7361.1 ± 11.1	6785.5	6873.0
CSD2R	1453.3 ± 5.5	1396.9 ± 11.2	1353.5	1402.7
DSD1R	2599.1 ± 5.5	2643.9 ± 11.4	2342.3	2397.1
DSD2R	1415.1 ± 5.7	1397.9 ± 11.2	1353.6	1402.7

If one summed up the worth of all of the single CRs, one would find this sum not to be equal to the worth of all CRs. The explanation is that there exists interference between control rods, and under the certain action of other CRs, the worth of a single one can be amplified or attenuated. The mathematical expression can be found in Eq. (2), where $\rho_{1,2...N}$ is the worth of all CRs, ρ_i is the worth of the investigated one and $\rho_{(1,2...N)-i}$ is the worth of all CRs except the investigated one.

$$A_{i} = \frac{\rho_{1,2..N} - \rho_{(1,2..N)-i}}{\rho_{i}}.$$
 (2)

If A_i <1, the worth of the given CR is attenuated and shadowing effects occur. Conversely, if A_i >1, there are anti-shadowing effects and the worth of the given CR is amplified. The results of the performed calculations can be found in Table 3.

Table 3 Results of control rod amplification factors

Control rod ID	SCALE6	MCNP5	DIF3D			
Control rod ID	E70 235G	E70 CE	KAFAX_E70	SBJ_E71		
CSD1	1.093 ± 0.005	1.097 ± 0.009	1.039	1.039		
CSD4	1.383 ± 0.025	1.348 ± 0.050	1.232	1.247		
DSD1	0.816 ± 0.008	0.810 ± 0.007	0.768	0.761		
DSD2	1.401 ± 0.025	1.306 ± 0.049	1.232	1.247		
CSD	0.963 ± 0.001	0.961 ± 0.002	0.944	0.942		
DSD	0.921 ± 0.002	0.916 ± 0.005	0.875	0.874		
CSD1R	0.969 ± 0.001	0.963 ± 0.003	0.944	0.942		
CSD2R	1.252 ± 0.008	1.220 ± 0.015	1.136	1.143		
DSD1R	0.816 ± 0.008	0.810 ± 0.007	0.768	0.761		
DSD2R	0.921 ± 0.002	1.218 ± 0.005	1.136	1.143		

We can conclude that the observed interference between CRs is not significant. The CSD and DSD systems are influenced only marginally. The 1st rings of the CSD and DSD systems are slightly attenuated and there is a small anti-shadowing effect in case of the second ring of both CSD and DSD systems. The strongest shadowing effect was observed for the central DSD1 assembly, which was caused by the presence of high worth CSD1-3 devices in the central region. The strongest anti-shadowing effect was found for CSD4, which is located in the region in which the neutron flux is pushed out from the centre due to the operation of DSD1 and CSD1-3 devices.

5.3 Sensitivity analyses

Sensitivity analysis of the ALLEGRO MOX core was performed using two computational tools. In the first case, the TSUNAMI-3D code was utilized using ENDF/B-VII 238 group XS data. Forward and adjoint transport calculations were carried out with KENO6 and the sensitivity coefficients were computed by the SAMS module of SCALE system. In the second case, self-developed perturbation PORK code was used, which is interconnected with the diffusion flux solver DIF3D and ZZ-KAFAX-E70. In the sensitivity analysis, it is common to ensure correctness of the sensitivity coefficients using Direct Perturbation calculation for the most important nuclides. Therefore, the DP calculation was carried out for a group of the most sensitive nuclides, which includes the majority of the fissile nuclides and the main nuclides of the structural materials. The results and nuclide affiliation to the material of the core are presented in Table 4.

Table 4 Energy and reaction integrated sensitivity coefficients for the most sensitive nuclides.

Material	Nuclide	Atom Density	Se	ensitivity (no-dim)		Error
Materiai	Nuclide	(atom/barn*cm)	DP	TSUNAMI-3D	PORK	(%)
Fuel	²³⁹ Pu	3.38250E-03	4.25266E-01	4.12350E-01	4.12812E-01	3.04
Fuel	²⁴¹ Pu	4.43250E-04	7.90059E-02	7.90059E-02 7.32350E-02		7.30
Fuel	^{238}U	1.67980E-02	-6.69112E-02	-6.61660E-02	-9.52177E-02	1.11
Fuel	²⁴⁰ Pu	1.55790E-03	3.88069E-02	3.64980E-02	3.50291E-02	5.95
Reflector *	⁵⁶ Fe	4.05280E-02	1.37285E-02	1.37110E-02	-1.71042E-02	0.13
Fuel	²³⁸ Pu	1.63770E-04	1.20460E-02	1.23260E-02	1.21718E-02	-2.32
Fuel	^{235}U	1.21830E-04	9.90339E-03	1.05700E-02	1.05833E-02	-6.73
Fuel	²⁴² Pu	4.35450E-04	5.82790E-03	6.48720E-03	6.07468E-03	-11.31
Reflector *	⁵² Cr	8.77190E-03	5.98321E-03	5.95130E-03	-3.74535E-03	0.53
Reflector *	⁵⁸ Ni	6.76710E-03	4.71109E-03	4.49750E-03	-7.31611E-03	4.53
Absorber	$^{10}\mathrm{B}$	6.05480E-02	-4.40663E-03	-4.18000E-03	-8.18243E-04	5.14
Reflector **	⁵⁶ Fe	3.79950E-02	3.36164E-03	3.67040E-03	-2.82496E-03	-9.18

^{*} material of the radial reflector, ** material of the axial reflector

The DP calculation was performed using the KENO6 code, where good agreement was reached with the results from TSUNAMI-3D calculation. The last column of Table 4 demonstrates the difference between the DP and TSUNAMI-3D calculations. None of the errors markedly exceeded 10%, which is acceptable. The situation is different in case of comparison of TSUNAMI-3D and PORK sensitivity coefficients. Sensitivity coefficients of the nuclides in structural materials calculated by the PORK code are negative where the sensitivity coefficients calculated by TSUNAMI-3D are strictly positive, but with a similar order of magnitude. When the integral sensitivity coefficients for structural materials were decomposed to reactions, scattering reactions were identified as the main contributor, with the same behaviour as was found for integral values. In Figure 4, the sensitivity profiles for elastic scattering are presented for three nuclides from structural materials (⁵⁶Fe, ⁵²Cr and ⁵⁸Ni), for which different integral sensitivity coefficients were obtained by calculation with TSUNAMI-3D, in Figure 4a), and PORK codes, in Figure 4-b). Despite the fact that sensitivity profiles also lay in the positive and negative regions, the importance of elastic scattering is the highest around incident neutron energy 1 MeV in both cases. This phenomenon has its origin in the core construction, where there is a lack of materials capable of significantly slowing down the neutrons. Therefore, the part of the fission neutrons which escaped from the fuel region is coming back with lower energy and their probability to cause fission is higher.

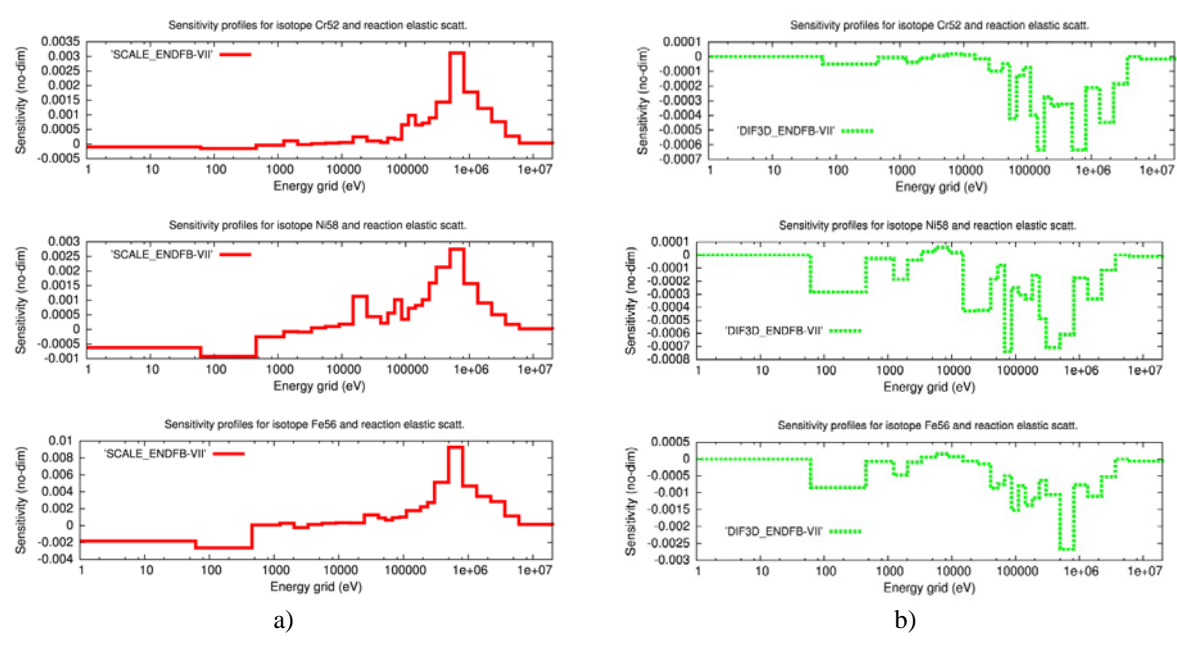


Figure 4 Sensitivity profiles for scattering reactions and chosen nuclides.

From the point of view of uncertainty calculations, the orientation of a sensitivity profile is not crucial, but in a case of optimization, interface effects between fuel and reflector or reactivity effects play a vital role.

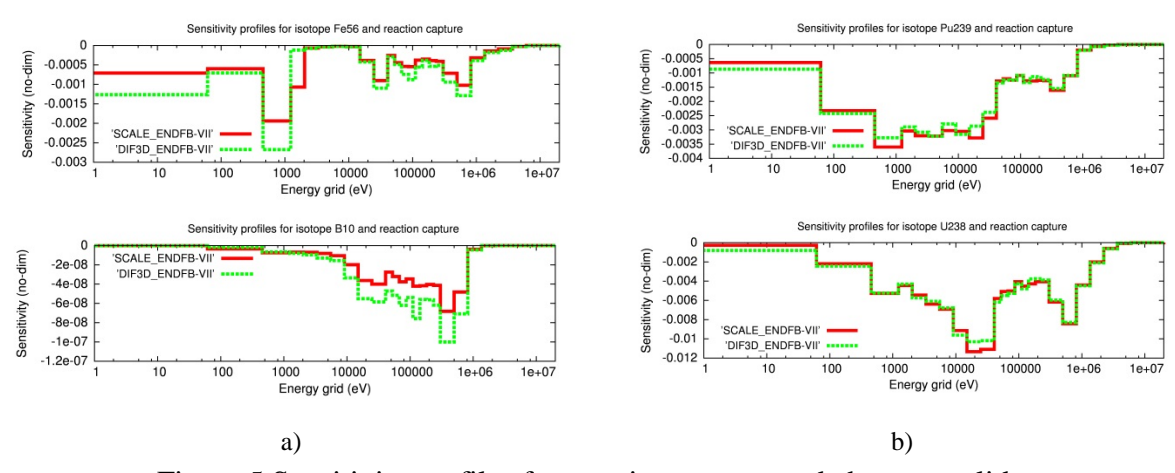


Figure 5 Sensitivity profiles for reaction capture and chosen nuclides

Another important effect is the leakage due to neutron capture. The sensitivity profiles for capture reaction and fissile nuclides (²³⁹Pu and ²³⁸U) are presented in Figure 5-b). The sensitivity profile for ²³⁸U reaches the highest absolute value in the resonance region, between energy levels of 1 to 100 keV, where the highest depression is shifted to the right part. Small depression can be also observed close to 1 MeV. This second (reverse) peak effect is probably related to the maximum of the neutron flux energy distribution. The second fissile nuclide, shown in Figure 5, is ²³⁹Pu. The absolute values of the sensitivities are two times lower, but the effective region of the profile is shifted to lower energies, where it is comparable to the sensitivity profile of ²³⁸U. The sensitivity profiles for ¹⁰B and ⁵⁶Fe capture reactions, presented in Figure 5-a), demonstrate the influence of parasitic absorption in structural materials and safety devices. During the flux calculation, the control and safety rods were in the upper position, since the sensitivity coefficient for capture on ¹⁰B were small.

Similarity assessment

The major source of uncertainty in the calculated response is due to uncertainties in evaluated nuclear data. Correlations as well as uncertainties in nuclear data can have a significant impact on the overall uncertainty in the calculated response; thus it is important to include them in the uncertainty analysis. By application of the TSUNAMI-IP utility, the neutronic similarity of ALLEGRO MOX core to the set of benchmarks was calculated and evaluated. The TSUNAMI-IP utility uses sensitivity data generated by TSUNAMI-1D/3D sequences and cross section-covariance data stored in the 44GRPCOV. ORNL developed a database of pre-calculated sensitivity profiles for several hundred critical benchmark experiments specified in the ICSBEP Handbook [10]. These sensitivities may be input into the TSUNAMI-IP utility, along with the calculated sensitivity profile of the application system. In our case, 494 benchmark experiments with various energy group structures were used. Three global integral indices [2] were used in the analysis to assess the similarity of ALLEGRO MOX neutronic core design (hereinafter application – index a) and a single experiment (e) on a system-wide basis for all nuclides and reactions. Each integral index is normalized such that a value of 1.0 represents complete similarity between application and specific benchmark experiment and the value of 0.0 indicated no similarity. The uncertainty of integral response ΔR (for instance, k_{eff}) by the use of XS sensitivity coefficients denoted by symbol S and XS and covariance matrix M can be evaluated by the sandwich formula:

$$\Delta R^2 = S_R M S_R^T \tag{3}$$

The diagonal elements of the resulting matrix defined by Eq.(3) represent the relative variance values for each system under consideration and the off-diagonal elements are the relative covariances between given experiments. These covariances, transformed to correlation coefficients (ck), describe the degree of correlation (coupling) of the uncertainties between the two specific systems. The E parameter given by Eq. (4) assesses the similarity between two systems based on the magnitude and shape of all sensitivity profiles. If the group-wise sensitivity data for all nuclides and reactions for each system are considered as a vector, the index E is the cosine of the angle between the sensitivity vectors.

$$E = S_a S_e^T / |S_a| |S_e| \tag{4}$$

The next G index assesses the similarity of two systems based on normalized differences in the

energy-dependent sensitivity data for fission, capture and scatter. The
$$G$$
 index is defined as follows:
$$G = 1 - \sum_{n} \sum_{x} \sum_{j} \left(S_{x,j}^{a,n} - S_{x,j}^{e',n} \right) / \sum_{n} \sum_{x} \sum_{j} \left(S_{x,j}^{a,n} \right), \tag{5}$$

where the symbol n stands for the number of application system nuclides, x represents the reaction and j is summation is performed over all energy groups. The nuclide-reaction specific partial integral index based on the same coverage criteria as G is denoted g. According to calculation, the relative standard deviation of ALLEGRO MOX $k_{\it eff}$ due to XS covariance data is 1.0404%. Table 5 lists the top 16 covariance matrices that contribute to k_{eff} uncertainty. These contributors represent more than 98% of the total uncertainty induced by XS data. The top contributor to application $\hat{k}_{\it eff}$ uncertainty is the $^{239}{
m Pu}$ nubar. This is due to large PuO₂ volume fraction (25.5%) in (U-Pu)O₂ MOX fuel and can be seen in Figure 6, consequently due to the high sensitivities above the 100 keV threshold. In case of ²³⁸U n,n' there are large negative sensitivities in the energy range above 1 MeV burdened with significant relative standard deviation of XS data (20 \div 35%). Although k_{eff} sensitivities to ²³⁹Pu n,gamma are in magnitude much smaller than ²³⁸U n,n' and ²³⁹Pu nubar, the uncertainty associated to XS data is large and vary between 5 to 45% in the relevant energy range.

Table 5 Uncertainty contribution in ALLEGRO MOX k_{eff}

No.	Covarian	ce Matrix	Uncertainty in k_{eff} (% $\Delta k/k$)	No	Covarian	Uncertainty in k_{eff} (% $\Delta k/k$)		
INO.	Nuclide-	Nuclide-	Due to the	No.	Nuclide-	Nuclide-	Due to the	
	Reaction	eaction Reaction Matrix			Reaction	Reaction	Matrix	
1	²³⁹ Pu nubar	²³⁹ Pu nubar	6.7999E-01	9	²³⁸ U n,gamma	²³⁸ U n,gamma	1.5155E-01	
2	²³⁸ U n,n'	²³⁸ U n,n'	5.0948E-01	10	²³⁸ U nubar	²³⁸ U nubar	1.1712E-01	
3	²⁴⁰ Pu nubar	²⁴⁰ Pu nubar	2.3377E-01	11	⁵⁶ Fe elastic	⁵⁶ Fe elastic	9.6235E-02	
4	²³⁹ Pu n,gamma	²³⁹ Pu n,gamma	2.3310E-01	12	⁵⁶ Fe n,gamma	⁵⁶ Fe n,gamma	7.5133E-02	
5	²³⁹ Pu chi	²³⁹ Pu chi	2.1225E-01	13	²⁴¹ Pu fission	²⁴¹ Pu fission	6.7164E-02	
6	²³⁸ Pu fission	²³⁸ Pu fission	2.0489E-01	14	²⁴⁰ Pu fission	²³⁹ Pu fission	5.8365E-02	
7	²³⁸ U elastic	²³⁸ U n,n'	1.9741E-01	15	⁵² Cr elastic	⁵² Cr elastic	5.4093E-02	
8	²³⁹ Pu fission	²³⁹ Pu fission	1.8240E-01	16	²³⁹ Pu n,n'	²³⁹ Pu n,n'	5.4073E-02	

Similarity assessment procedure identified three groups of potential experiments, where c(k)coefficients got over 0.4. However, only one experiment (MIX-COMP-FAST-001-001) reached c(k)greater than 0.9, as can be seen in Figure 6-a).

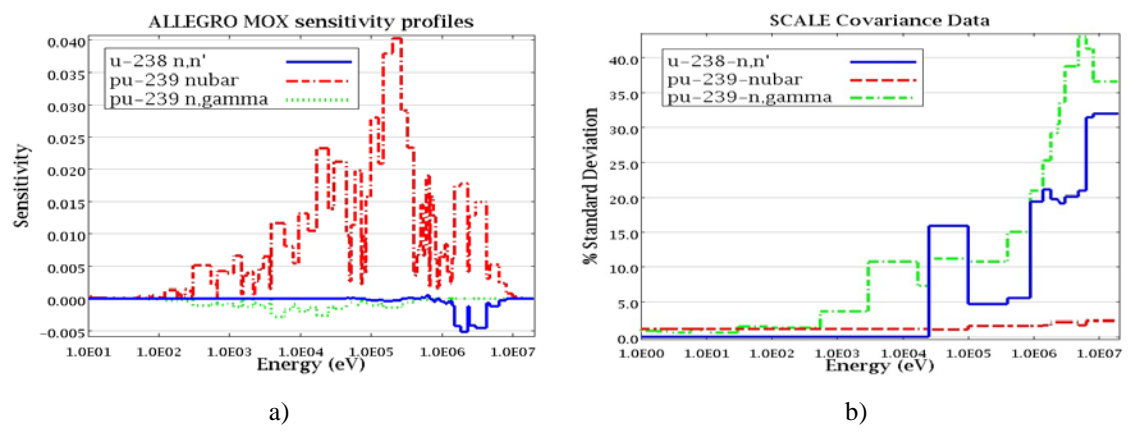


Figure 6 Application sensitivity profiles and covariance data

Good similarity results are mainly driven by the type of fuel (MOX) and the fuel cladding material. Although the E coefficient reaches quite a high value (0.95), the big portion (25%) of sensitivity profiles is uncovered (G) by this experiment. This is mainly caused by different construction materials and coolants used in adopted models resulting to the dissimilar neutron spectra. The short characteristics of other identified experiments are shown in Table 6.

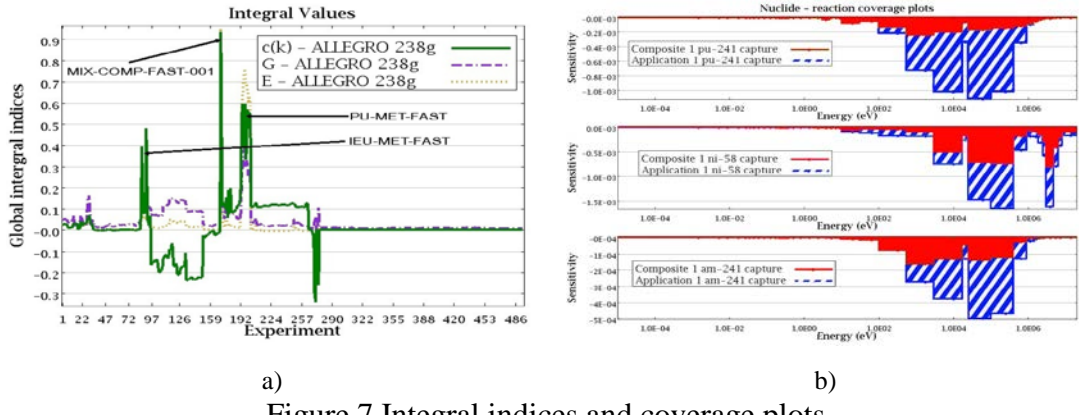


Figure 7 Integral indices and coverage plots

Pu Metal

From Table 6 we can conclude that the majority of identified experiments, with exception of MIX-COMP-FAST-001-001, are simple plutonium metal systems. The average fission group energy in these systems is quite high due to the absence of moderator and structural materials (over 1 MeV). Because of their simplicity, the *G* value gets very low for all cases.

ID	ICSBEP ID	Fissile material	Moderator	Average Fission Group Energy	Neutron Flux > 100 keV	Capture > 100 keV	Cladding	Reflector	c(k)	E	G
171	MIX-COMP-FAST-001-001	MOX	Na	99.8 keV	57%	22%	SS	Depl. U	0.93	0.95	0.75
197	PU-MET-FAST-008-001	Pu Metal	-	1.08 MeV	95%	80%	-	Th	0.60	0.68	0.30
194	PU-MET-FAST-002-001	Pu Metal	-	1.28 MeV	97%	85%	-	-	0.60	0.62	0.30
199	PU-MET-FAST-018-001	Pu Metal	-	913 keV	92%	57%	-	Be	0.57	0.67	0.30
201	PU-MET-FAST-023-001	Pu Metal	-	1.17 MeV	97%	83%	-	Gr	0.56	0.63	0.26
202	PU-MET-FAST-024-001	Pu Metal	-	647 keV	95%	45%	-	PE	0.54	0.62	0.27
193	PU-MET-FAST-001-001	Pu Metal	-	1.28 MeV	97%	86%	-	-	0.54	0.60	0.26
200	PU-MET-FAST-022-001	Pu Metal	_	1.26 MeV	97%	86%	_	_	0.54	0.60	0.26

Table 6 Integral indices for similar experiments in relation to ALLEGRO MOX core

The values of g indices for the nuclide – reaction pairs, having a great impact on the active core neutron balance, are given in Table 7.

ID	²³⁸ U	²³⁸ U	²³⁹ Pu	²³⁸ U	²⁴⁰ Pu	⁵⁶ Fe	⁵⁸ Ni	²³⁸ U	²⁴¹ Pu	¹⁶ O	²⁴¹ Am
ID	capture	total	capture	n,n'	capture	capture	capture	scatter	capture	capture	capture
171	1.00	0.99	0.98	0.99	0.46	0.90	0.47	0.96	0.20	1.00	0.35

Table 7 Results of nuclide-reaction specific partial integral index g

The data presented in Table 7 highlights the nuclide-reaction pairs which are not sufficiently covered by MIX-COMP-FAST-001-001 experiment. Figure 7-b) shows the coverage of the most problematic nuclide – reaction sensitivity profiles of all experiments involved in calculation. The hashed area of sensitivity profiles highlights the importance of experimental verification of used nuclear data of energies in the interval between 100 keV and 1 MeV.

6. Conclusion

196

PU-MET-FAST-006-001

In this study, the neutronic performance of the ESNII+ ALLEGRO MOX core was investigated. The stochastic MCNP and SCALE and the deterministic DIF3D codes were used with various XS libraries. In case of SCALE, the MG treatment was used and the lowest discrepancy with the MCNP CE calculation was found for 238 group XSs with cell calculations. In case of DIF3D, both ZZ_KAFAX_E70 and SBJ_620G_E71 MATXS cross section libraries demonstrated good performance. It was discovered that although the XS libraries differed in terms of excess reactivity, the deviation for the CR worth calculation was not significant. The results of the CR interference analysis showed that there exist some shadowing and anti-shadowing effects between the CRs, but they are not significant. The calculation of LMV factors identified an existence of local neutronic zones. This phenomenon should be studied further in future studies. By way of conclusion it can be said that it is advantageous to perform the ALLEGRO core calculations by DIF3D, since the precision is comparable

with Monte Carlo ones, calculation time is much shorter and it is not burdened with statistical uncertainties. The sensitivity analysis of the ALLEGRO MOX core was performed using two different computational tools. The correctness of integral sensitivity coefficients was investigated by DP calculation for TSUNAMI-3D sensitivity coefficients, where satisfactory conformity was achieved. The comparison of integral sensitivity coefficients calculated by TSUNAMI-3D and PORK code identified some discrepancies for elastic scattering reaction, which was also confirmed by visual comparison of corresponding sensitivity profiles. Other sensitivity coefficients and profiles show a good agreement for both codes and can serve as a base for following analyses. Finally, the overall uncertainty of k_{eff} was calculated to be consistent with previous results. Similarity assessment identified 9 partly-comparable experiments where only one reached c(k) and E values over 0.9. However the Global Integral Index G still remains low (0.75) and cannot be deemed sufficient. The total uncertainty of calculated k_{eff} induced by XS data is, according to our calculation, 1.04%. The main contributors to this uncertainty are ²³⁹Pu nubar and ²³⁸U inelastic. The additional margin from uncovered sensitivities was determined to be 0.28%. The identified low number of similar experiments prevents the use of advanced XS adjustment and bias estimation methods. More experimental data is needed and presented results may serve as a basic step in development of necessary critical assemblies. Although exact data is not presented in the paper, faster 44 energy group calculation gives almost the same results in similarity analysis in comparison to more complex 238 group calculation.

7. Acknowledgement

This study has been financially supported by the Slovak Research Development Agency No. APVV-0123-12, Scientific Grant Agency of the Ministry of Education of Slovak Republic and the Slovak Academy of Sciences No. VEGA 1/0796/13 and by the project Research Centre ALLEGRO, OPVaV-2013/2.2/09-RO - ITMS No. 26220220198.

8. References

- [1] Generation IV International Forum, "A Technology Roadmap for Generation IV Energy Systems", USA, 2002.
- [2] E. Temesvári, "ALLEGRO core specification", Deliverable D6.6.1-2, Issued by CER, 2014.
- [3] ORNL, "SCALE: A Comperhensive Modeling and Simulation Suite for Nuclear Safety Analysis and Design", ORNL/TM-2005/39, 2011.
- [4] LANL, "MCNP A General N Particle Transport Code", LA-UR-03-1987, Los Alamos, USA, 2003.
- [5] ORNL, "DIF3D: Code System Using Variational Nodal Methods and Finite Difference Methods to Solve Neutron Diffusion and Transport Theory Problems", RSIC CCC-784, 2011.
- [6] MacFarlane, R. E., et al., "TRANSX 2: A code for Interfacing MATXS Cross-Section Libraries to Nuclear Transport Codes", Los Alamos National Laboratory, LA-12312-MS, Los Alamos, USA, 1992.
- [7] D.H. Kim et all., "Validation Tests of the Multigroup Cross Section Libraries for Fast Reactors", PHYSOR -2006, Vancouver, BC, Canada, 2006.
- [8] M. B, Chadwick et al., "ENDF/B-VII.0: Next Generation Evaluated Nuclear Data Library for Nuclear Science and Technology", *Nuclear Data Sheets*, vol. 107, no. 12, 2006, p. 2931.
- [9] R E. MacFarlane and A.C. Kahler, "Methods for Processing ENDF/B-VII with NJOY", *Nuclear Data Sheets*, Vol.111, LA-RU-10-04652, 2010, pp.2739-2890
- [10] OECD Nuclear Energy Agency, International Handbook of Evaluated Criticality Safety Benchmark Experiments, (2010)